BJR

https://doi.org/10.1259/bjr.20210534

Received: 28 April 2021 | Revised: 08 October 2021 | Accepted: 23 October 2021

Cite this article as:
Li X, Ma Q, Nie P, Zheng Y, Dong C, Xu W. A CT-based radiomics nomogram for differentiation of renal oncocytoma and chromophobe renal cell carcinoma with a central scar-matched study. *Br J Radiol* 2021; **95**: 20210534.

FULL PAPER

A CT-based radiomics nomogram for differentiation of renal oncocytoma and chromophobe renal cell carcinoma with a central scar-matched study

[1]XIAOLI LI, [2]QIANLI MA, [1]PEI NIE, [3]YINGMEI ZHENG, [1]CHENG DONG and [1]WENJIAN XU

[1]Department of Radiology, The Affiliated Hospital of Qingdao University, Qingdao, Shandong, China
[2]Department of Radiology, Qingdao Municipal Hospital, Qingdao, Shandong, China
[3]Health Management Center, The Affiliated Hospital of Qingdao University, Qingdao Shandong, China

Address correspondence to: Dr Wenjian Xu
E-mail: *xuwenjian3769@126.com*

Objective: Pre-operative differentiation between renal oncocytoma (RO) and chromophobe renal cell carcinoma (chRCC) is critical due to their different clinical behavior and different clinical treatment decisions. The aim of this study was to develop and validate a CT-based radiomics nomogram for the pre-operative differentiation of RO from chRCC.

Methods: A total of 141 patients (84 in training data set and 57 in external validation data set) with ROs (n = 47) or chRCCs (n = 94) were included. Radiomics features were extracted from tri-phasic enhanced-CT images. A clinical model was developed based on significant patient characteristics and CT imaging features. A radiomics signature model was developed and a radiomics score (Rad-score) was calculated. A radiomics nomogram model incorporating the Rad-score and independent clinical factors was developed by multivariate logistic regression analysis. The diagnostic performance was evaluated and validated in three models using ROC curves.

Results: Twelve features from CT images were selected to develop the radiomics signature. The radiomics nomogram combining a clinical factor (segmental enhancement inversion) and radiomics signature showed an AUC value of 0.988 in the validation set. Decision curve analysis revealed that the diagnostic performance of the radiomics nomogram was better than the clinical model and the radiomics signature.

Conclusions: The radiomics nomogram combining clinical factors and radiomics signature performed well for distinguishing RO from chRCC.

Advances in knowledge: Differential diagnosis between renal oncocytoma (RO) and chromophobe renal cell carcinoma (chRCC) is rather difficult by conventional imaging modalities when a central scar was present.
A radiomics nomogram integrated with the radiomics signature, demographics, and CT findings facilitates differentiation of RO from chRCC with improved diagnostic efficacy.
The CT-based radiomics nomogram might spare unnecessary surgery for RO.

BACKGROUND

Renal oncocytoma (RO) is the second most common benign renal tumor, accounting for 3–7% of all renal lesions.[1,2] It is a rare, slow-growing tumor with a favorable prognosis that is usually diagnosed incidentally during a routine examination. Therapeutic strategies for RO involve conservative management.[3] Chromophobe renal cell carcinoma (chRCC), an aggressive renal cell neoplasm, is the third most common histological subtype of renal cell carcinoma (RCC) after clear cell renal carcinoma and papillary cell renal carcinoma. Possible surgical treatment options include partial or radical nephrectomy.[4] Although chRCC is considered less aggressive than other renal cell neoplasms, it has metastatic potential and can cause death.[1] RO and chRCC originate from the epithelial cells of the proximal renal tubule. In addition to their common cellular origin, RO and chRCC share similar imaging manifestations including a central scar.[1] Given the common morphological and imaging manifestations and their different clinical treatments, accurate pre-operative differentiation between RO and chRCC is challenging for personalized treatment, especially for those with a central scar.

Many studies have attempted to distinguish RO from chRCC by performing multiphase enhanced computed tomography (MECT) or MRI using qualitative and quantitative measures. Wu et al discovered that spoken-wheel-like enhancement and segmental enhancement inversion (SEI)

helped differentiate RO from chRCC.[4] Choi et al found that the appearance of a central stellate scar and higher mean HU values in the nephrogenic phase were useful for differentiating RO from chRCC.[1] Schieda et al indicated that SEI was a specific imaging finding of RO with highly variable sensitivity (80%).[5] Demirovic et al reported the presence of a fibrous capsule distinguished between RO and chRCC.[6] However, the enhancement degree of CT and the difference in CT value between RO and chRCC are markedly influenced by subjective factors. Other studies showed that many MRI sequences such as signal intensity ratios, fast spin-echo T2 signal intensities, wash-in values, and diffusion-weighted imaging were diagnostic parameters for discriminating between the two tumor types.[7,8] Although these studies have contributed to distinguishing RO from chRCC using multiple imaging modalities, none focused on the differentiation of RO from chRCC when a central scar was present. Conventional imaging modalities are unable to reliably differentiate between RO and chRCC; therefore, a non-invasive and accurate method is urgently needed to help achieve a diagnosis pre-operatively.

Radiomics, an innovation of image technology, can change medical images into mineable data sets via the high-throughput extraction of quantitative features.[9] It has shown promising results in terms of evaluating tumor characteristics, differential diagnosis, and improving clinical decision-making.[10] Many studies have investigated radiomics features for the differentiation of RCC from benign renal tumors, including RO.[9,11,12] However, to the best of our knowledge, few studies have focused on radiomics for the differential diagnosis of RO and chRCC, especially for those with a central scar.

The aim of this study was to develop and validate a predictive CT-based radiomics nomogram model to differentiate RO from chRCC using tri-phasic enhanced CT when a central scar is present.

METHODS AND MATERIALS

Patients

This retrospective study was approved by the Institutional Review Board of two hospitals and the need for informed consent was waived due to the nature of the study. Considering the rarity of RO and the consistent imaging protocol and scanner used for contrast-enhanced CT, the enrollment period was from January 2010 to March 2021. The inclusion criteria were as follows: (1) RO or chRCC confirmed by post-operative surgical pathology reports; (2) central scar present in the RO and chRCC groups proven by histopathological findings. Central scar was defined as a central area of fibrous connective tissue with bands of fibrosis radiating toward the periphery of the lesion[13]; and (3) pre-operative tri-phasic contrast-enhanced CT taken within 2 weeks before surgery. The exclusion criteria were as follows: (1) image quality was unsatisfactory for tumor identification; (2) clinical factors were incomplete or missing; and (3) patients received anti cancer treatment before surgery. Finally, 84 patients with ROs (n = 28; 9 men and 19 women; mean age, 58.25 ± 14.22 years) or chRCCs (n = 56; 29 men and 27 women; mean age,

Figure 1. The flow diagram of the study population. chRCC, chromophobe renal cell carcinoma; RO, renal oncocytoma

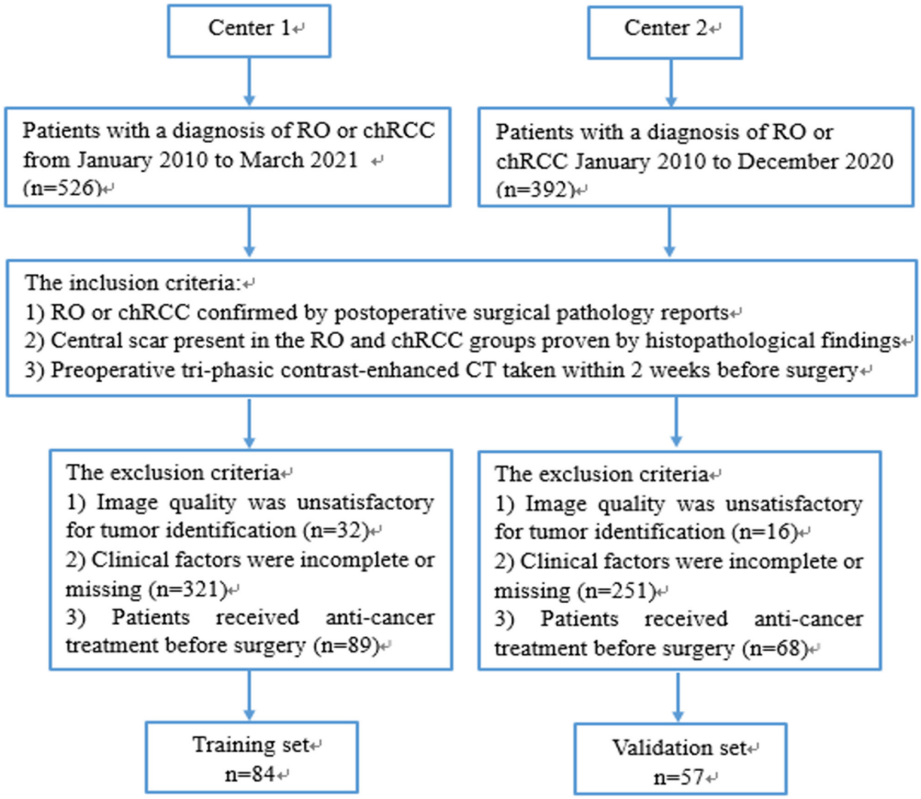

Table 1. CT scan protocols

	Center 1 (Training set)	Center 2 (Validation set)
Manufacturer	Siemens Healthcare, Berlin, Germany	GE Healthcare, Chicago, IL
Scanner model	Somatom Sensation 64	Discovery CT 750 HD
Sequence	Axial	Axial
Tube voltage (kV)	120	120
Tube current	200 mAs	250–400 mA (using automatic modulation)
Gantry rotation time (s)	0.5	0.5
Detector collimation (mm)	64 × 0.6	64 × 0.625
Matrix	512 × 512	512 × 512
Thickness of slice (mm)	2.5	2.5
Phase of contrast enhancement	Three phases	Three phases
Corticomedullary phase (s)	35–40	35–40
Nephrographic phase (s)	90	90
Excretory phase (min)	7–9	7–9

53.02 ± 12.98 years) were enrolled into the training data set. **An external validation data set** of 57 patients with RO (n = 19; 11 men and 8 women; mean age, 57.16 ± 11.37 years) or chRCC (n = 38; 12 men and 26 women; mean age, 54.53 ± 11.07 years) from another medical center was acquired with the same criteria from January 2010 to December 2020. The flow diagram of the study population is presented in Figure 1. Demographic information including gender and age was derived from admission records.

CT image acquisition

The CT scan protocols are detailed in Table 1. Non-ionic intravenous contrast material (80–100 ml iopromide, Ultravist 370; Bayer Schering Pharma, Berlin, Germany) was administered with a power injector at a rate of 3.0 ml s^{-1}. The corticomedullary phase (CP), nephrographic phase (NP), and excretory phase (EP) were acquired at 35–40 s, 90 s, and 7–9 min, respectively, after the start of the contrast injection.

CT feature evaluation

Two abdominal radiologists with 16- and 18 years' experience reassessed the CT features independently. They evaluated the following CT features respectively and blindly to the pathology reports: laterality (left or right), location (cortical side/medullary side), SEI (present or absent, defined as two differently-enhancing segments on CP with the relative degree of enhancement reversed on the NP),[14] necrosis (present or absent, defined as a lesion with an irregular and heterogeneous hypodensity area with no enhancement on contrast-enhanced CT), cystic components (present or absent, defined as a round and homogeneous hypodensity area with no enhancement on contrast-enhanced CT), hemorrhage (present or absent), calcification (present or absent), fat (present or absent), and perirenal fascia thickening (present or absent, defined as a focal lesion with a well-defined interface between fat and tumor).[15] When disagreement was present, a consensus would be reached by discussion.

Figure 2. The tumor segmentation on the axial slice was showed in (**a**) RO of a 59-year-old female located in the right kidney (b-c). A central scar was displayed in the central area of the tumor (b, black arrow). The perirenal fascia thickening was displayed in b (white arrow). SEI was featured in the tumor. The surrounding area of the tumor shows wash in on CP (b) and wash-out on EP (c), whereas the central scar shows progressive enhancement on EP. CP, corticomedullary phase; EP, excretory phase; RO, renal oncocytoma; SEI, segmental enhancement inversion.

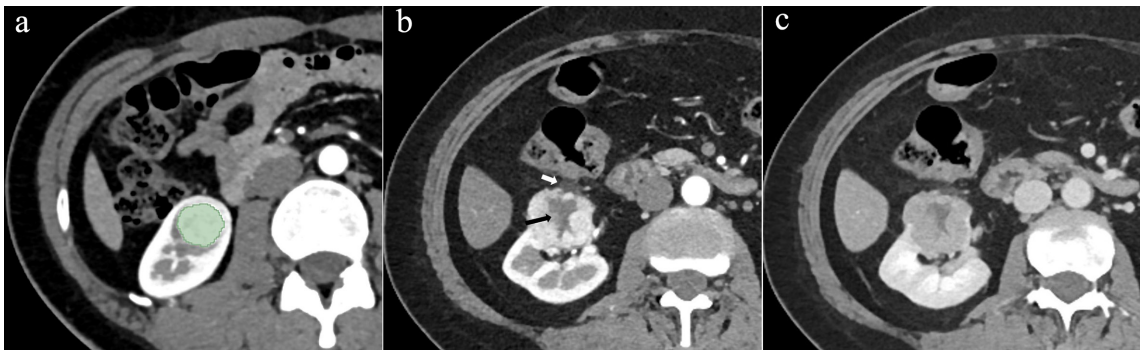

Clinical model building

Differences in clinical data and CT imaging features between RO and chRCC were analyzed by univariate analysis in the training data set. Then, significant variables from the univariate analysis as inputs were selected to build the clinical model by multiple logistic regression analysis. Odds ratios (OR) and 95% confidence intervals (CIs) were acquired for each independent risk factor.

Image segmentation and extraction of radiomics features

Three-dimensional (3D) tumor segmentation of regions of interest (ROIs) was performed by a junior radiologist (Radiologist 1) and a senior radiologist (Radiologist 2) via 3D Slicer software (v. 4.10.2, https://www.slicer.org). ROIs were manually delineated in the tumors' outermost boundaries slice by slice on axial CP, NP, and EP images, while avoiding adjacent blood vessels and normal tissue. An example of the manual segmentation is shown in Figure 2a.

851 radiomics features were acquired from the ROIs of 3D tumor segmentation on each phase using 3D Slicer software (Pyradiomics v. 2.2.0), including 107 original and 744 wavelet-filtered features. The details and formulas for radiomics features are explained at https://pyradiomics.readthedocs.io/en/latest/features.html and in a previous radiomics study.[16] To ensure the conservation of scale when deriving the 3D features, CT images were discretized with a bin width of 25 HU and resampled at a spatial resolution of $1 \times 1 \times 1\,mm^3$ using linear interpolation.[17] Z-score normalization were conducted to guarantee the repeatability of the results. Overall, 2553 radiomics features were obtained.

Inter - and intra class correlation coefficients (ICCs, (2,1))[18] were performed to indicate the reproducibility of radiomics features. 30 cases of CT images (15 RO and 15 chRCC) were selected randomly. ROI segmentation was conducted independently by Radiologist 1 and Radiologist 2 to assess the inter observer reproducibility. To estimate the intra observer reproducibility, Radiologist 1 performed the same procedure 2 weeks later. An ICC greater than 0.75 was considered good agreement. If strong agreement was achieved for most features, Radiologist 1 then performed the image segmentation on the remaining cases.

Radiomics signature building

The selection of radiomics features with good agreement (ICCs > 0.75) was completed using one-way analysis of variance (ANOVA). Significant variables from the ANOVA were included for least absolute shrinkage and selection operator (LASSO)[19] to select the most valuable features for building the radiomics signature in the training set. 10-fold cross-validation via the minimum criteria was performed in LASSO regression. A radiomics score (Rad-score) was calculated for each case, with the respective coefficients weighted by the LASSO logistic regression model.

Radiomics nomogram development and performance assessment of different models

To predict the probabilities of a diagnosis between RO and chRCC, a radiomics nomogram model was created by incorporating the significant variables related to clinical factors and Rad-score. A radiomics nomogram score (Nomo-score) was calculated based on the significant clinical factors and Rad-score by multiple logistic regression analysis in the training and validation data sets. Calibration curves were plotted to investigate the

Table 2. Clinical factors of the training and validation sets

Clinical factors	Training set (n = 84)			Validation set (n = 57)	
	RO (n = 28)	chRCC (n = 56)	P	RO (n = 19)	chRCC (n = 38)
Gender (M/F)	9/19	29/27	0.088	11/8	12/26
Age, year	58.25 ± 14.22	53.02 ± 12.98	0.985	54.43 ± 16.19	55.26 ± 12.75
Laterality (Left/Right)	11/17	35/21	0.044	6/13	21/17
Location (cortical side/medullary side)	15/13	17/39	0.039	8/11	13/25
SEI (present/ absent)	21/7	13/43	<0.001	17/2	4/34
Necrosis (present/ absent)	0/28	1/55	1.000	0/19	4/34
Cystic components (present/ absent)	0/28	4/52	0.296	2/17	4/34
Hemorrhage (present/ absent)	0/28	2/54	0.550	0/19	1/37
Calcification (present/ absent)	0/28	7/49	0.090	1/18	2/36
Fat (present/ absent)	0/28	1/55	1.000	0/19	0/38
Perirenal fascia thickening (present/ absent)	17/11	13/43	<0.001	14/5	12/26

F, female; M, male; RO, renal oncocytoma; SEI, segmental enhancement inversion;chRCC, chromophobe renal cell carcinoma.
P: the p-value of comparison between RO and chRCC in training set; Numerical data are presented as mean ± standard deviation, categorical data as numbers (n).

Figure 3. Radiomics feature extraction using the LASSO regression model (a, b). (**a**) 10-fold cross-validation via the minimum error criterion was used for tuning parameter (λ) selection in LASSO. The optimal values of the LASSO tuning parameter (λ) are indicated by the dotted vertical lines, and a value λ of 0.091 was selected. (**b**) LASSO coefficient profiles of the 2391 radiomics features. A coefficient profile plot was generated *vs* the selected log λ value using 10-fold cross-validation. 12 radiomics features with non-zero coefficients were selected. LASSO, least absolute shrinkage and selection operator.

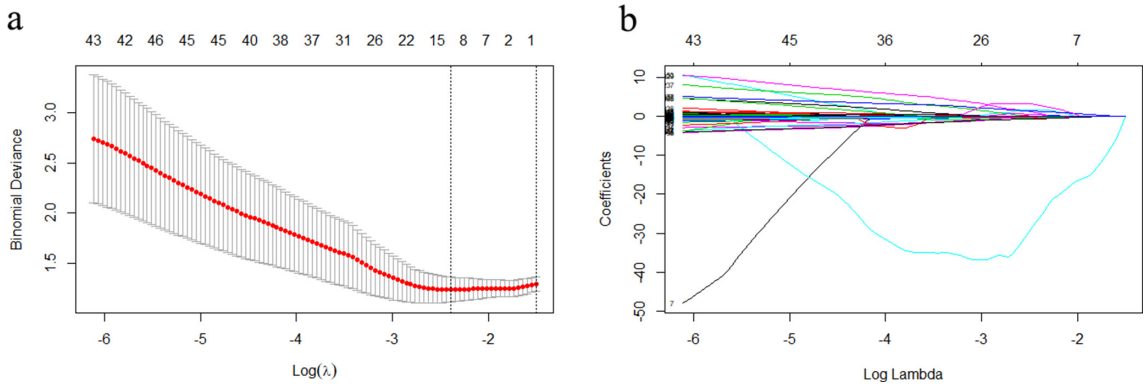

calibration of the nomogram graphically. On the basis of the area under the receiver operator characteristic (ROC) curve (AUC), the performance of the three models to differentiate RO from chRCC was evaluated in the two data sets. The clinical utility of the nomogram was estimated by decision curve analysis (DCA), which incorporates the three decision curves (clinical factors, radiomic signature, and radiomics nomogram) in the validation set by calculating the net benefits for a range of threshold probabilities.

Statistical analysis

Statistical tests were conducted with SPSS v. 20.0 (SPSS, Chicago, IL) and R software (v. 3.3.3 (https://www.r-project.org). The level of significance was set at a two-sided $p < 0.05$. The details of the statistical analyses are presented in the Supplementary Material.

RESULTS

Clinical model building

Data of clinical factors in the training and validation data sets are presented in Table 2. Significant differences were found between RO and chRCC including laterality (right), location (cortical side), SEI, and perirenal fascia thickening (Figure 2b–2c) in the training data set by univariate analysis (both $p < 0.05$). The four selected clinical factors were used for multivariable logistic regression analyses. The p values were 0.072, 0,079, < 0.001, and 0.223, respectively. Only SEI was selected as an independent predictor for the clinical model of RO (OR, 9.508; 95% CI, 2.897 ~ 31.206).

Radiomics signature building

Overall, 2553 radiomics features were extracted from the MECT images and 2408 features with ICC values > 0.750 had good

Table 3. Radiomics features selection results

Variables	Tri-phasic enhanced CT	Radiomics feature name
A	CP	Zone Entropy. GLSZM. Wavelet-HLH
B	NP	Correlation. GLCM. Wavelet-LLL
C	EP	Correlation. GLCM. Wavelet-LLL
D	CP	Maximum. First order. Wavelet-LHL
E	CP	Idn. GLCM. Wavelet-LLL
F	CP	Correlation. GLCM. Wavelet-LLL
G	NP	Mean. First order. Wavelet-LHL
H	NP	Imc2. GLCM. Wavelet-LLL
I	NP	Median. First order. Original
J	EP	Maximum. First order. Wavelet-LHL
K	EP	Mean. First order. Wavelet-LHL
L	EP	Maximum Probability. GLCM. Wavelet-HHH

GLCM: Gray level co-occurrence matrix; GLSZM: Gray level size zone matrix;CP: Corticomedullary phase; NP: Nephrographic phase; EP: Excretory phase.

Table 4. The results of Rad-score and Nomo-score in the training and validation set

	Training set			Validation set		
	RO	chRCC	*P1*	RO	chRCC	*P2*
Rad-score	0.101 ± 0.129	−1.221 ± 0.074	<0.001	−0.036 ± 0.093	−1.045 ± 0.082	<0.001
Nomo-score	3.953 ± 0.785	−5.162 ± 0.458	<0.001	3.547 ± 0.584	−4.484 ± 0.501	<0.001

Rad-score: radiomics score; Nomo-score: nomogram score.; RO: renal oncocytoma; chRCC: chromophobe renal cell carcinoma.
Numerical data are presented as mean ± standard deviation.
P1: the *p*-value of comparison between RO and chRCC in training set;
P2: the *p*-value of comparison between RO and chRCC in validation set.

agreement (Supplementary Table 1). The radiomics signatures of the remaining samples were extracted by Radiologist 1. Then, 2391 radiomics features that displayed significant differences between RO and chRCC ($p < 0.050$) were selected by ANOVA and included in LASSO to acquire the most valuable factors. Finally, 12 radiomics features were confirmed as candidates for building the radiomics signature by LASSO and the best-tuned regularization parameter λ of 0.091under the minimum criteria was determined by 10-fold cross-validation (Figure 3). The formula of Rad-score is as follows: Rad-score = 18.83282106 A*0.32734208 + B*1.70840119 + C*0.06423074-D*0.22868788-E*25.96391469 + F*0.85245442 - G*0.01802623 + H*0.4357135 + I*1.31378975 - J*0.54437267 - K*0.03603238 + L*2.86918717. The variables A to L, which represent significant radiomic features for predicting RO, are shown in Table 3. The Rad-scores revealed significant differences between RO and chRCC in the training and validation data sets (Table 4).

Radiomics nomogram development and assessment of the performance of the three models

A radiomics nomogram incorporating the selected clinical factors (SEI) and Rad-score was constructed via multivariable logistic regression analysis (Figure 4). In the present study, the Nomo-score was calculated using the following equation: Nomo-score = 1.312+M*2.733 + R*5.821 (M = SEI; R = Rad-score). There were significant differences in Nomo-scores between RO and chRCC in the training and validation data sets (Table 4).

Using the calibration curve, we confirmed a good calibration in the training and validation data sets (Figure 5a and b). The diagnostic performances of the three models are presented in Table 5. ROC curves of the three models in the training and validation data sets are shown in Figure 6a and b. The radiomics nomogram showed considerably better discrimination between RO and chRCC than the clinical model in the training ($p < 0.001$) and external validation data sets ($p = 0.016$).

The decision curve indicated that the radiomics nomogram added greater overall net benefit compared with the clinical model and radiomics signature in differentiating between RO and chRCC in the validation data set across most of the range of reasonable threshold probabilities. The DCA for the three models in the validation data set is shown in Figure 7.

DISCUSSION

In the present study, we built and validated three models based on tri-phasic enhanced CT, including clinical model, radiomics signature, and radiomics nomogram. Finally, with external validation, a radiomics nomogram integrating SEI and radiomics signature had the best diagnostic performance for differentiating RO from chRCC among the three models. The AUC, sensitivity, specificity, and accuracy of the radiomics nomogram were significantly better than those of the clinical model and radiomics signature (0.988, 89.5%, 97.4%, and 94.7% in the validation data sets, respectively).

Figure 4. The radiomics nomogram incorporating SEI and Rad-score was constructed in the training data set. A point value on the "Points" horizontal axis can be obtained from the "SEI" axis and "Rad. Score" axis, respectively. The sum of the two values corresponds to a point value on the "Total points" axis. The point value on the "Risk" axis, which corresponds to the "Total points", reflects the risk of a patient suffering RO. RO, renal oncocytoma; SEI, segmental enhancement inversion.

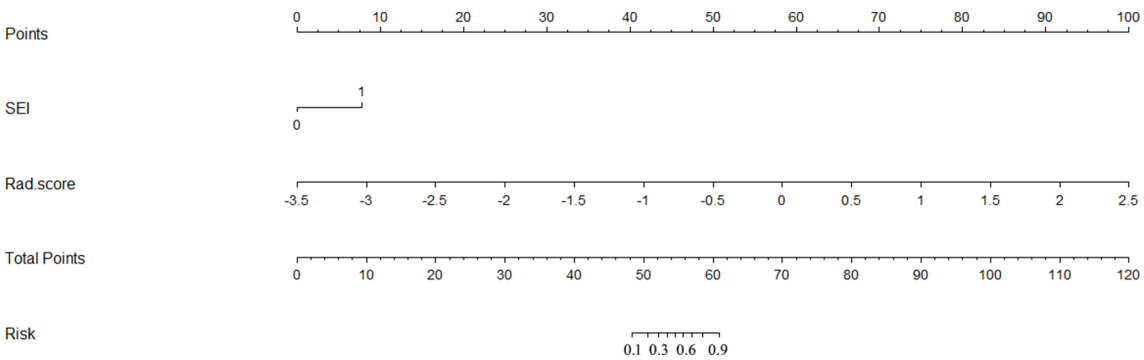

Figure 5. Calibration curves for the radiomics nomogram in the training (a) and validation (b) data sets. Calibration curves indicate the goodness-of-fit of the nomogram. The 45° straight line indicates the perfect match between the actual (Y-axis) and nomogram-predicted (X-axis) probabilities. A closer distance between two curves represents higher accuracy.

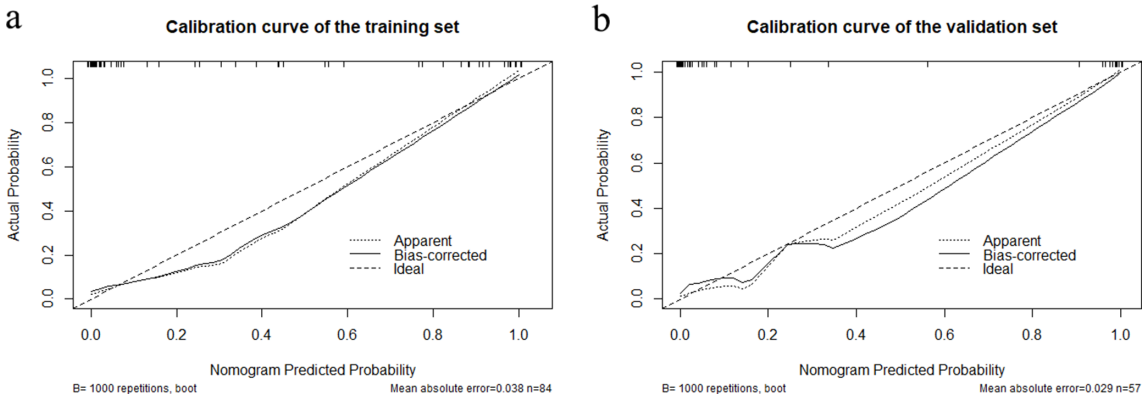

Differentiating RO from chRCC is important for selecting appropriate therapeutic strategies and avoiding unnecessary interventions. A large amount of clinical and imaging information is required for the correct differentiation of RO from chRCC.[1,4,20] 10 clinical factors were used in the present study, including gender, age, laterality, location, SEI, necrosis, cystic components, hemorrhage, calcification, fat, and perirenal fascia thickening. There was a significant SEI predominance in the RO group compared with the chRCC group, as previously reported.[5]

As an artificial intelligence, radiomics is widely used for the differential diagnosis of benign and malignant renal tumors.[21–26] It enables the non-invasive profiling of tumor heterogeneity by extracting high throughput quantitative data from images to aid clinical decision-support. Previous investigations suggested that CT/MR-based radiomics might be used to differentiate RO from RCC. Siva et al[27] created a random forest model to categorize RCC from benign renal legions. Forty cases of RCC (including 20 clear cell RCC (ccRCC), 20 papillary RCC (pRCC), and 40 cases of benign renal legion (including 20 RO and 20 renal cysts) were included, and the random forest model successfully distinguished the four lesion types with high sensitivity: 89% for RO, 91% for ccRCC, and 100% for pRCC and renal cysts. However, chRCC was not examined as a common type of RCC. Yu et al[12] investigated a CT-based texture analysis model to differentiate between different renal tumors (n = 119), including 46 ccRCC, 41 pRCC, 22 chRCC, and 10 RO. The texture analysis included histogram and gray-level features. The histogram feature median allowed the discrimination of chRCC from RO with an AUC of 0.88, whereas the gray-level features were poor-to-fair discriminators

Table 5. Diagnostic performance of the clinical model, radiomics signature and radiomics nomogram

Model	Cut-off	AUC (95% CI)	Sensitivity %	Specificity %	Accuracy %	TPR%	FPR%	TNR%	FNR%
Training set (n = 84)									
Clinical model	−1.815	0.759 (0.646–0.872)	75.0	76.8	76.2	61.8	38.2	86.0	14.0
Radiomics signature	−0.662	0.966 (0.933–0.998)	82.1	92.9	89.3	85.2	14.8	91.2	8.8
Radiomics nomogram	−0.168	0.979 (0.954–1.000)	89.3	96.4	94.0	92.6	7.4	94.7	5.3
Validation set (n = 57)									
Clinical model	−1.815	0.895 (0.796–0.993)	89.5	73.7	78.9	81.0	19.0	94.4	5.6
Radiomics signature	−0.545	0.957 (0.904–1.000)	84.2	94.7	91.2	88.9	11.1	92.3	7.7
Radiomics nomogram	0.190	0.988 (0.966–1.000)	89.5	97.4	94.7	94.4	5.6	94.9	5.1

CI: confidence interval; Data in the parentheses are raw data.; TPR, True Positive Rate; FPR, False positive Rate; TNR, True Negative Rate; FNR, False Negative Rate.

Figure 6. The ROC curves of the clinical model, the radiomics signature and the radiomics nomogram for training (a) and validation sets (b). ROC, receiver operating characteristic.

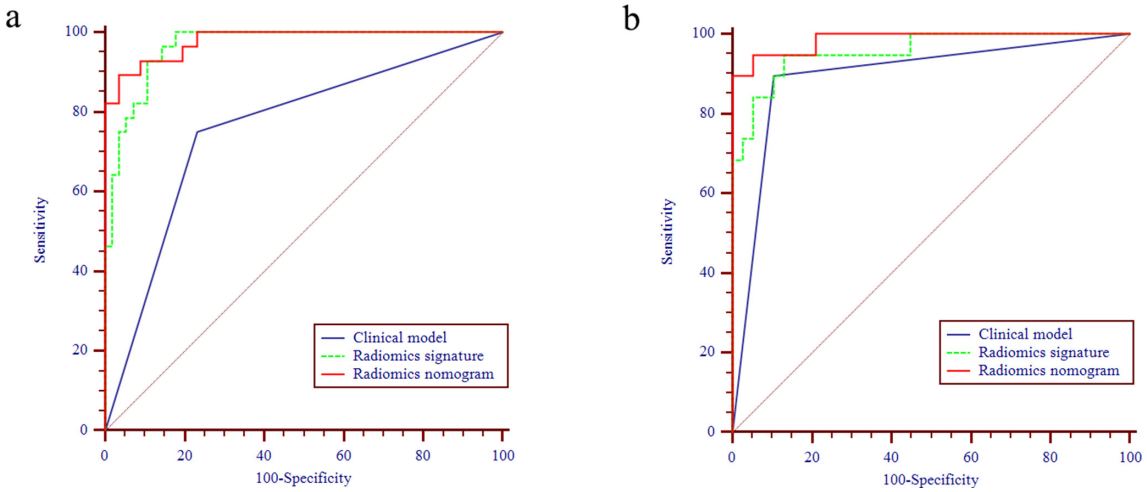

of chRCC from RO. Sun et al[28] developed and validated CT- and MRI-based radiologic-radiomic machine learning models to distinguish benign and malignant solid renal masses. 254 RCC (including 190 ccRCC, 38 chRCC, and 26 pRCC) and 36 cases of benign renal tumors (including 10 RO and 26 fat-poor angioleiomyolipomas) were analyzed. The radiologic-radiomic machine learning models showed a high specificity (91.7%) for pRCC and chrRCC from fat-poor angioleiomyolipomas and RO, although the sensitivity was only 73.4%. Apart from the relatively low sensitivity, the discrimination of RO and chRCC was not separately investigated in the study due to the small samples of chRCC and RO. A similar MR-based texture model was created by Razik et al[29] to discriminate between RCC and RO and lipid-poor angiomyolipoma. They found the best parameter to differentiate RCC from RO was mean at spatial scaling factor (0 mm) on DWI (b = 1000). However, only six cases of RO were enrolled and the clinical factors of the patients were not analyzed. Li et al[30] developed a CT-based radiomics method that focused on the differential diagnosis of RO from chRCC with five machine learning classifications. 17 RO and 44 chRCC were included, and 1029 features were extracted from radiomics features. All five classifiers displayed good diagnostic performance with AUC values greater than 0.850. However, the sample of RO was relatively small and clinical factors (including traditional imaging features) were not included in the analysis. In the present study, we enrolled 47 RO and 94 chRCC, and all features were extracted from the radiomics signature. The diagnostic performance with AUC of the clinical model, the radiomics signature and the radiomics

Figure 7. Decision curve analysis for three models. The y-axis reveals the net benefit; x-axis shows threshold probability. The red line, green line, and blue line indicate net benefit of the clinical model, the radiomics signature, and the radiomics nomogram, respectively. The radiomics nomogram had a higher overall net benefit in differentiating ROs from chRCCs than the other two models. Simple diagnoses such as all ROs patients (gray line) or all chRCCs patients (black line) across the full range of threshold probabilities at which a patient would be diagnosed as ROs. chRCC, chromophobe renal cell carcinoma; RO, renal oncocytoma.

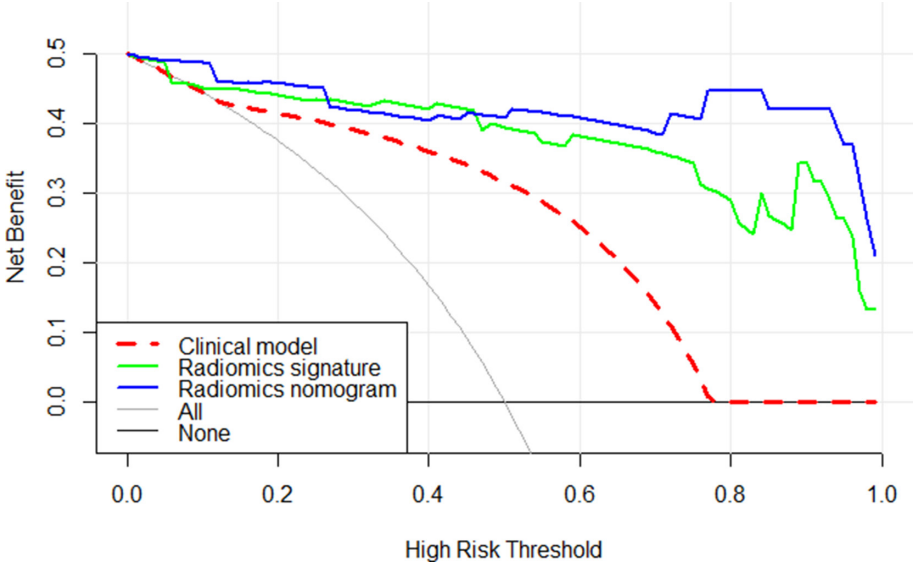

nomogram was 0.895, 0.957, 0.988, respectively, in the validation set.

Our study had several differences and improvements compared with the previous radiomics studies. **First**, we focused on the differential diagnosis of RO from chRCC in patients with a central scar because this often causes misdiagnosis in routine clinical practice. **Second**, as a relatively rare renal tumor, **47 RO patients** were enrolled in the present study. To the best of our knowledge, this is the largest number of samples used to differentiate RO from chRCC based on radiomics signature. **Third**, an external validation data set was used to assess the diagnostic performance of different models. The AUC of the radiomics nomogram in the validation data set was 0.988, which demonstrated a good diagnostic performance of the model in the validation data set. This also indicates a good predictive value on unfitting new data, and further demonstrated its good predictive ability and robustness.

Our study had several limitations

First, owing to the retrospective nature of the study, selection bias was present and we developed the radiomics signature using only tri-phasic contrast-enhanced CT. Other imaging modalities, including ultrasound, dynamic contrast-enhanced MRI, and diffusion-weighted imaging, could also be used to develop a combined radiomics nomogram model by incorporating tri-phasic contrast-enhanced CT. Second, two different CT scanners were used in the present study, although similar parameters were used for CT scans. Third, only patients who underwent nephrectomy were included in this study. This could bias the selection of patients. Those patients, who displayed typical imaging appearance of RO and underwent renal mass biopsy, should also be included in the future study. Fourth, pre-operative tri-phasic contrast-enhanced CT was performed in our study. A single contrast phase should be investigated whether it can provide similar diagnostic information to all phases combined. Another limitation of the present study is the limited sample size relative to the number of radiomics features which were used to derive the radiomics model.

CONCLUSIONS

We constructed and validated a tri-phasic enhanced CT-based radiomics nomogram, which combined clinical factors and radiomics features. It achieved favorable pre-operative and predictive efficacy for the differentiation of RO from chRCC. The clinical use of the radiomics nomogram as a new non-invasive and quantitative method remains to be tested.

ACKNOWLEDGEMENTS

None

CONTRIBUTORS

1 Guarantor of integrity of the entire study: Cheng Dong, Wenjian Xu.
2 Study concepts and design: Cheng Dong, Wenjian Xu and Xiaoli Li.
3 Literature research: Xiaoli Li, Qianli Ma, Pei Nie, and Yingmei Zheng.
4 Clinical studies: Cheng Dong, Wenjian Xu, Xiaoli Li, Qianli Ma and Pei Nie.
5 Experimental studies / data analysis: N/A.
6 Statistical analysis: Cheng Dong, Xiaoli Li.
7 Manuscript preparation: Xiaoli Li, Qianli Ma.
8 Manuscript editing: Cheng Dong and Wenjian Xu.

COMPETING INTERESTS

The authors declare that they have no any conflicts of interest in their manuscript.

FUNDING

None

PATIENT CONSENT

The need for informed consent was waived due to the retrospective nature of the study.

ETHICS APPROVAL

This retrospective study was approved by the Institutional Review Board of the Affiliated Hospital of Qingdao University and Qingdao Municipal Hospital.

DISCLOSURE

Agree

REFERENCES

1. Choi JH, Kim JW, Lee JY, Han WK, Rha KH, Choi YD, et al. Comparison of computed tomography findings between renal oncocytomas and chromophobe renal cell carcinomas. *Korean J Urol* 2015; **56**: 695–702. doi: https://doi.org/10.4111/kju.2015.56.10.695
2. Stec R, Grala B, Maczewski M, Bodnar L, Szczylik C. Chromophobe renal cell cancer--review of the literature and potential methods of treating metastatic disease. *J Exp Clin Cancer Res* 2009; **28**: 134. doi: https://doi.org/10.1186/1756-9966-28-134
3. Scialpi M, Martorana E, Rondoni V, Eissa A, Sherbiny AE, Bevilacqua L, et al. Value of triphasic MDCT in the differentiation of small renal cell carcinoma and oncocytoma. *Urologia* 2017; **84**: 244–50. doi: https://doi.org/10.5301/uj.5000256
4. Ljungberg B, Albiges L, Abu-Ghanem Y, Bensalah K, Dabestani S, Fernández-Pello S, et al. European association of urology guidelines on renal cell carcinoma: the 2019 update. *Eur Urol* 2019; **75**: 799–810. doi: https://doi.org/10.1016/j.eururo.2019.02.011
5. Schieda N, McInnes MDF, Cao L. Diagnostic accuracy of segmental enhancement inversion for diagnosis of renal oncocytoma at biphasic contrast enhanced CT: systematic review. *Eur Radiol* 2014; **24**: 1421–9. doi: https://doi.org/10.1007/s00330-014-3147-4
6. Demirović A, Cesarec S, Spajić B, Tomas D, Bulimbasić S, Milosević M, et al. Can

renal oncocytoma be distinguished from chromophobe renal cell carcinoma by the presence of fibrous capsule? *Virchows Arch* 2010; **456**: 85–9. doi: https://doi.org/10.1007/s00428-009-0868-x
7. Akın IB, Altay C, Güler E, Çamlıdağ İlkay, Harman M, Danacı M, et al. Discrimination of oncocytoma and chromophobe renal cell carcinoma using MRI. *Diagn Interv Radiol* 2019; **25**: 5–13. doi: https://doi.org/10.5152/dir.2018.18013
8. Zhong Y, Wang H, Shen Y, Guo A, Wang J, Kang S, et al. Diffusion-Weighted imaging versus contrast-enhanced MR imaging for the differentiation of renal oncocytomas and chromophobe renal cell carcinomas. *Eur Radiol* 2017; **27**: 4913–22. doi: https://doi.org/10.1007/s00330-017-4906-9
9. Lubner MG. Radiomics and artificial intelligence for renal mass characterization. *Radiol Clin North Am* 2020; **58**: 995–1008. doi: https://doi.org/10.1016/j.rcl.2020.06.001
10. Guo J, Liu Z, Shen C, Li Z, Yan F, Tian J, et al. MR-based radiomics signature in differentiating ocular adnexal lymphoma from idiopathic orbital inflammation. *Eur Radiol* 2018; **28**: 3872–81. doi: https://doi.org/10.1007/s00330-018-5381-7
11. Sun X-Y, Feng Q-X, Xu X, Zhang J, Zhu F-P, Yang Y-H, et al. Radiologic-Radiomic machine learning models for differentiation of benign and malignant solid renal masses: comparison with Expert-Level radiologists. *American Journal of Roentgenology* 2020; **214**: W44–54. doi: https://doi.org/10.2214/AJR.19.21617
12. Yu H, Scalera J, Khalid M, Touret A-S, Bloch N, Li B, et al. Texture analysis as a radiomic marker for differentiating renal tumors. *Abdom Radiol* 2017; **42**: 2470–8. doi: https://doi.org/10.1007/s00261-017-1144-1
13. Giambelluca D, Pellegrino S, Midiri M, Salvaggio G, et al. The "central stellate scar" sign in renal oncocytoma. *Abdom Radiol* 2019; **44**: 1942–3. doi: https://doi.org/10.1007/s00261-019-01899-3
14. Kim JI, Cho JY, Moon KC, Lee HJ, Kim SH. Segmental enhancement inversion at biphasic multidetector CT: characteristic finding of small renal oncocytoma. *Radiology* 2009; **252**: 441–8. doi: https://doi.org/10.1148/radiol.2522081180
15. Omiyale AO, Carton J. Renal oncocytoma with vascular and perinephric fat invasion. *Ther Adv Urol* 2019; **11**: 1756287219884857. doi: https://doi.org/10.1177/1756287219884857
16. Coroller TP, Grossmann P, Hou Y, Rios Velazquez E, Leijenaar RTH, Hermann G, et al. Ct-Based radiomic signature predicts distant metastasis in lung adenocarcinoma. *Radiother Oncol* 2015; **114**: 345–50. doi: https://doi.org/10.1016/j.radonc.2015.02.015
17. Hong JH, Jung J-Y, Jo A, Nam Y, Pak S, Lee S-Y, et al. Development and validation of a Radiomics model for differentiating bone islands and osteoblastic bone metastases at abdominal CT. *Radiology* 2021; **299**: 626–32. doi: https://doi.org/10.1148/radiol.2021203783
18. Erratum to "A Guideline of Selecting and Reporting Intraclass Correlation Coefficients for Reliability Research" [J Chiropr Med 2016;15(2):155-163. *J Chiropr Med* 2017; **16**: 346. doi: https://doi.org/10.1016/j.jcm.2017.10.001
19. Alhamzawi R, Ali HTM, . The Bayesian adaptive LASSO regression. *Math Biosci* 2018; **303**: 75–82. doi: https://doi.org/10.1016/j.mbs.2018.06.004
20. Amin J, Xu B, Badkhshan S, Creighton TT, Abbotoy D, Murekeyisoni C, et al. Identification and Validation of Radiographic Enhancement for Reliable Differentiation of CD117(+) Benign Renal Oncocytoma and Chromophobe Renal Cell Carcinoma. *Clin Cancer Res* 2018; **24**: 3898–907. doi: https://doi.org/10.1158/1078-0432.CCR-18-0252
21. Nie P, Yang G, Wang Z, Yan L, Miao W, Hao D, et al. A CT-based radiomics nomogram for differentiation of renal angiomyolipoma without visible fat from homogeneous clear cell renal cell carcinoma. *Eur Radiol* 2020; **30**: 1274–84. doi: https://doi.org/10.1007/s00330-019-06427-x
22. Xi IL, Zhao Y, Wang R, Chang M, Purkayastha S, Chang K, et al. Deep learning to distinguish benign from malignant renal lesions based on routine MR imaging. *Clin Cancer Res* 2020; **26**: 1944–52. doi: https://doi.org/10.1158/1078-0432.CCR-19-0374
23. Kocak B, Durmaz ES, Erdim C, Ates E, Kaya OK, Kilickesmez O. Radiomics of renal masses: systematic review of reproducibility and validation strategies. *AJR Am J Roentgenol* 2020; **214**: 129–36. doi: https://doi.org/10.2214/AJR.19.21709
24. Said D, Hectors SJ, Wilck E, Rosen A, Stocker D, Bane O, et al. Characterization of solid renal neoplasms using MRI-based quantitative radiomics features. *Abdom Radiol* 2020; **45**: 2840–50. doi: https://doi.org/10.1007/s00261-020-02540-4
25. Ma Y, Cao F, Xu X, Ma W. Can whole-tumor radiomics-based CT analysis better differentiate fat-poor angiomyolipoma from clear cell renal cell caricinoma: compared with conventional CT analysis? *Abdom Radiol* 2020; **45**: 2500–7. doi: https://doi.org/10.1007/s00261-020-02414-9
26. Uhlig J, Leha A, Delonge LM, Haack A-M, Shuch B, Kim HS, et al. Radiomic features and machine learning for the discrimination of renal tumor histological subtypes: a pragmatic study using Clinical-Routine computed tomography. *Cancers* 2020; **12**: 301016 10 2020. doi: https://doi.org/10.3390/cancers12103010
27. Raman SP, Chen Y, Schroeder JL, Huang P, Fishman EK. Ct texture analysis of renal masses: pilot study using random forest classification for prediction of pathology. *Acad Radiol* 2014; **21**: 1587–96. doi: https://doi.org/10.1016/j.acra.2014.07.023
28. Sun X-Y, Feng Q-X, Xu X, Zhang J, Zhu F-P, Yang Y-H, et al. Radiologic-Radiomic machine learning models for differentiation of benign and malignant solid renal masses: comparison with Expert-Level radiologists. *AJR Am J Roentgenol* 2020; **214**: W44–54. doi: https://doi.org/10.2214/AJR.19.21617
29. Razik A, Goyal A, Sharma R, Kandasamy D, Seth A, Das P, et al. Mr texture analysis in differentiating renal cell carcinoma from lipid-poor angiomyolipoma and oncocytoma. *Br J Radiol* 2020; **93**: 20200569. doi: https://doi.org/10.1259/bjr.20200569
30. Li Y, Huang X, Xia Y, Long L, et al. Value of radiomics in differential diagnosis of chromophobe renal cell carcinoma and renal oncocytoma. *Abdom Radiol* 2020; **45**: 3193–201. doi: https://doi.org/10.1007/s00261-019-02269-9